Amyloid peptide Aβ40 inhibits aggregation of Aβ42: Evidence from molecular dynamics simulations

Man Hoang Viet and Mai Suan Li

Citation: J. Chem. Phys. **136**, 245105 (2012); doi: 10.1063/1.4730410
View online: http://dx.doi.org/10.1063/1.4730410
View Table of Contents: http://jcp.aip.org/resource/1/JCPSA6/v136/i24
Published by the American Institute of Physics.

Amyloid peptide Aβ_{40} inhibits aggregation of Aβ_{42}: Evidence from molecular dynamics simulations

Man Hoang Viet and Mai Suan Li[a)]
Institute of Physics, Polish Academy of Sciences, Al. Lotnikow 32/46, 02-668 Warsaw, Poland

(Received 24 October 2011; accepted 7 June 2012; published online 29 June 2012)

Effects of amyloid beta (Aβ) peptide Aβ_{40} on secondary structures of Aβ_{42} are studied by all-atom simulations using the GROMOS96 43a1 force field with explicit water. It is shown that in the presence of Aβ_{40} the beta-content of monomer Aβ_{42} is reduced. Since the fibril-prone conformation **N*** of full-length Aβ peptides has the shape of beta strand-loop-beta strand this result suggests that Aβ_{40} decreases the probability of observing **N*** of Aβ_{42} in monomer state. Based on this and the hypothesis that the higher is the population of **N*** the higher fibril formation rates, one can expect that, in agreement with the recent experiment, Aβ_{40} inhibit fibril formation of Aβ_{42}. *It is shown that the presence of Aβ_{40} makes the salt bridge D23–K28 and fragment 18–33 of Aβ_{42} more flexible providing additional support for this experimental fact*. Our estimation of the binding free energy by the molecular mechanics-Poisson-Boltzmann surface area method reveals the inhibition mechanism that Aβ_{40} binds to Aβ_{42} modifying its morphology. © *2012 American Institute of Physics*. [http://dx.doi.org/10.1063/1.4730410]

I. INTRODUCTION

Alzheimer's disease (AD) is the most common form of dementia among the senior population and is characterized pathologically by the progressive intracerebral accumulation of β-amyloid (Aβ) peptides. These peptides are proteolytic byproducts of the Aβ protein precursor and are most commonly composed of 40 (Aβ_{40}) and 42 (Aβ_{42}) amino acids. Aβ peptides appear to be unstructured in their monomer state but aggregate to form fibrils with an ordered cross β-sheet pattern.[1–4] The assembly of Aβ peptides is an important event in the development of AD. Although Aβ_{40} is about 10 times more abundant than Aβ_{42} *in vivo*, Aβ_{42} is significantly more neurotoxic than Aβ_{40}.[5] Increasing evidence from recent studies indicates that soluble Aβ_{42} oligomers such as dimer,[6] trimer,[7] 12mer[8] as well as mature fibrils are the toxic agent.[9–11] In contrast, the Aβ_{42} monomer is not toxic.[5] Therefore, any agent that prevents Aβ_{42} monomers from aggregation can play a protective role against the development of AD by reducing the generation of neurotoxic species.

The role of Aβ_{40} in AD has not been well understood. There are two possible scenarios that this peptide either inhibits aggregation or degrades aggregates of Aβ_{42}. Recent studies have suggested its protective role showing that reduced levels of Aβ_{40} are correlated with accelerated onset of dementia.[12,13] However, at the molecular level, it is not clear how Aβ_{40} executes its protective function in AD pathogenesis. One of possible scenarios is that Aβ_{40} inhibits fibril formation of Aβ_{42} as evidenced from *in vivo*[14,15] and *in vitro* experiments.[15–18] This interesting problem has not been, however, considered theoretically and our goal is to understand the mechanism of inhibition of Aβ_{42} aggregation by Aβ_{40} using molecular dynamics (MD) simulations. Because the estimation of fibril assembly rates of full-length Aβ peptides is computationally prohibited, we try to achieve this goal using the hypothesis that the higher are aggregation rates the higher is the population of the fibril-prone conformation **N*** in monomer state.[19,20] One of the examples supporting this hypothesis is that Aβ_{42} peptides aggregate into β-sheet fibril much faster than Aβ_{40} ones[21] because the former has higher beta-content (β-content) in the monomer state.[20,22]

Using the GROMOS96 43a1 force field[23] with explicit water we have performed conventional MD simulations of monomer Aβ_{40}, Aβ_{42}, and one mixed system of Aβ_{40} and Aβ_{42}. This mixed system will be refereed to as Aβ_{40+42}. It should be noted that previous computational studies[24–27] focus either on Aβ_{40} or Aβ_{42} dimer but the interaction between Aβ_{40} and Aβ_{42} has not been considered. We have found that Aβ_{40} reduces the β-content of Aβ_{42} compared to the monomer case. *The flexibility of the salt bridge D23-K28 and fragment 18-33 of Aβ_{42} gets enhanced in the presence of Aβ_{40}*. These results suggests that, in agreement with the experiment,[18] Aβ_{40} inhibits the fibril formation of Aβ_{42}. In order to get more insight on the mechanism of inhibition we have estimated the binding free energy ΔG_{bind} of Aβ_{40} to "receptor" Aβ_{42} using the molecular mechanics-Poisson-Boltzmann surface area (MM-PBSA) method.[28] Since ΔG_{bind} followed from our simulations is negative, one can conclude that in agreement with the experiment,[16] Aβ_{40} interferes with Aβ_{42} aggregation through the binding mechanism.

II. MATERIALS AND METHODS

A. Structures of amyloid peptides used as starting configurations for simulations

The NMR structures of full-length Aβ_{40} (protein data bank (PDB) code: 1BA4 (Ref. 29) and Aβ_{42} (PDB code: 1Z0Q (Ref. 30), taken from the PDB, are rich in helix as they

a)masli@ifpan.edu.pl.

have been solved in micellar solutions. To obtain unstructured structures for starting configurations in simulations they were heated up to $T = 500$ K. The 5 ns MD simulations were carried at this temperature until one gets random coil structures using the GROMOS96 43a1 force field.[31]

B. Fibril-prone conformation N*

Structure **N*** is defined as the structure of the peptide/protein in the fibril state.[19,20] In the Aβ_{42} case first 16 residues are disordered and omitted. Therefore, **N*** is the structured part Aβ_{17-42} (PDB entry: 2BEG (Ref. (4)) (see Fig. S1 in the supplementary material (SM)[77]) that includes the loop (27–30) and two fragments (1–26) and (31–42). For Aβ_{40} **N*** is defined as the ordered fragment Aβ_{9-40} because the 8 residues are disordered and excluded from fibril structure construction.[32] The loop region of **N*** is extended over residues 24–28, while two fragments are (1–23) and (29–40). The structure of fragment Aβ_{9-40} has been provided by Professor R. Tycko (Fig. S1 in SM[77]).

C. MD simulations

The GROMACS 4.5.4 package[23] was used to run MD simulations with the GROMOS96 43a1 force field[31] and the simple point charge (SPC) water model.[33] This force field was proved to be useful in studying aggregation of peptides[34–36]). The equations of motion were integrated by using a leap-frog algorithm[37] with a time step of 2 fs. The LINCS algorithm[38] was used to constrain the length of all bonds. The van der Waals (vdW) forces were calculated with a cutoff of 1.4 nm, and particle-mesh Ewald method[39] was employed to treat the long-range electrostatic interactions. The non-bonded interaction pair-list was updated every 10 fs with the cutoff of 1 nm.

For monomers 300 ns isothermal-isobaric ensemble (NPT) MD runs have been carried out at $T = 300$ K starting from random coil structures (Fig. 1, upper panel) obtained at high T as described above. The $5.8 \times 5.8 \times 5.8$ nm^3 cubic box, which contains about 6120 water molecules, has been used for simulation. In the united-atom GROMOS model the number of atoms is equal to 388 and 403 for Aβ_{40} and Aβ_{42}, respectively. For the mixed system Aβ_{40+42} four independent 500 ns runs have been carried out starting from initial configurations shown in middle and lower panels of Fig. 1, where structures of two monomers are the same as in upper panel. Positions of two monomers were randomly placed in the $6.9 \times 6.9 \times 6.9$ nm^3 cubic box. The total number of water molecules is about 10560.

D. MM-PBSA method

This part is available in SM.[77]

E. Equilibration

We monitor time dependence of energy E of the system. The equilibrium is reached if this dependence gets saturation. In addition we calculate the specific heat $C_P = (\langle E^2\rangle - \langle E\rangle^2)/(k_B T^2)$ at $T = 300$ K in equilibrium for the entire and half MD run. If values of C_P obtained for short (between t_{eq} and $t_{full}/2$) and long (between t_{eq} and t_{full}) trajectory coincide then the system can be considered as equilibrated. Here, t_{eq} and t_{full} are equilibration time and time of the entire MD run.

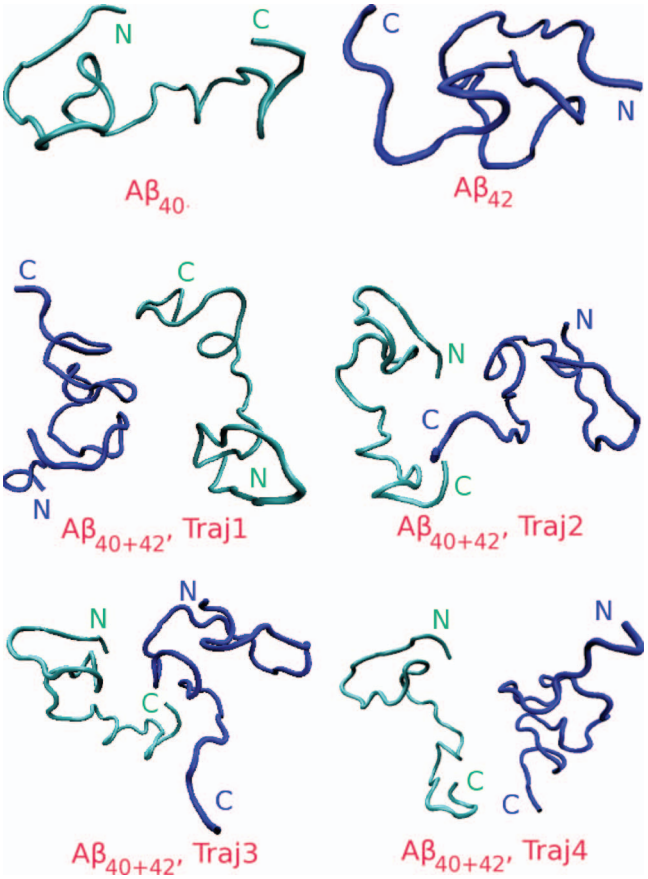

FIG. 1. Starting conformations used in MD simulations for monomer Aβ_{40} and Aβ_{42} (upper panel), and four trajectories of the mixed system Aβ_{40+42} (middle and lower panel). Positions of two peptides in the mixed system have been randomly placed in boxes with the periodic boundary conditions. Both peptides in all starting configurations are unstructured. Plots have been made using visual molecular dynamics (VMD) software.[48]

F. Tools and measures used in the structure analysis

1. Contact maps

The time evolution of formation of side chain–side chain (SC–SC) and hydrogen bond (HB) contacts was monitored. A SC–SC contact is formed if the distance between the centers of mass of two residues is $\leq$6.5 Å. HB is formed if distance between donor D and acceptor A is $\leq$3.5 Å and the angle D–H–A is $\geq$135°.

2. Secondary structures

Secondary structure (beta, helix, and coil) contents of peptides were calculated using the STRIDE algorithm.[40,41]

III. RESULTS AND DISCUSSIONS

A. Monomers

The Aβ peptides have very high propensity to aggregation and for this reason it has not yet been possible to study the full-length peptides in water solution. In water but at low pH fragments of Aβ adopt mainly coil structures.[42,43] To avoid aggregation experiments have been performed in a mixture of water and organic solvents such as micellar solutions,[29,44] trifluoroethanol,[45,46] or hexafluoroisopropanol.[30,47] Under these conditions the full-length Aβ peptides display substantial helical structure.

The question about the structure of Aβ peptides in aqueous environment remains open as different groups have reported different results on their secondary structures.[20,22,36,49,50] Thus, it is worth to further explore this problem. In our previous paper[36] secondary structures of Aβ_{40} and Aβ_{42} were probed using the GROMOS96 43a1 force field and 300 ns MD simulations starting from their PDB structures (1BA4 and 1Z0Q are PDB codes for Aβ_{40} and Aβ_{42}, respectively). It was found that the most probable structure of Aβ_{40} contains roughly 60%, 30%, and 10% of *RC*, α- and β-content, respectively. This result is in accord with the United Residues (UNRES) force field[50] but conflicts with other groups[20,22,49] reporting the lower helix content. To see if the initial configurations change our previous conclusion about secondary structures[36] we have performed 500 ns conventional MD simulations for monomers using random coil structures (Fig. 1, upper panel) as starting configurations.

1. C_α chemical shifts of Aβ_{40} and Aβ_{42}

To check if our canonical 500 ns MD simulations generate structures relevant to experimental ones, we calculate chemical shifts δ_{sim} and compare them with experimental values δ_{sim}. The time dependence of energy (Fig. S2 in SM[77]) shows that both monomers reach equilibrium after about t_{eq} =110 ns and 70 ns for monomer Aβ_{40} and Aβ_{42}, respectively. We have also calculated C_P for time intervals $[t_{\text{eq}}, t_{\text{full}}/2]$ and $[t_{\text{eq}}, t_{\text{full}}]$ (see SM[77]) for both trajectories, where $t_{\text{full}} = 500$ ns. The results obtained for these intervals coincide (Table S1 in SM[77]) indicating that the systems reach equilibrium at t_{eq}. Therefore, snapshots collected during last 390 ns and 430 ns are used for calculation of C_α chemical shifts δ_{sim} using the SHIFT program.[52,53] The 500 ns canonical MD (CMD) produces remarkable agreement with results obtained by replica exchange MD (REMD)[20] experiments[51] for δ_{sim} of individual residues of Aβ_{40} (Fig. S3 in SM[77]) and Aβ_{42} (Fig. S4 in SM).[77] Moreover, our *in silico* result obtained for C_α atoms is correlated with the NMR experiments of Hou *et al.*[51] (Figs. 2(a) and 2(b)) with correlation level $R = 0.98$ and 0.99 for Aβ_{40} and Aβ_{42}, respectively. Using the REMD and recently improved assisted model building with energy refinement (AMBER) force field PARM99SB[54] Yang and Teplow[20] have obtained $R = 0.994$ and 0.995 for Aβ_{40} and Aβ_{42}, respectively. The high correlation has been also observed for atoms N_α (results not shown). It seems that the strong correlation between our theoretical data and those produced by experiment and REMD indicate that our 500 ns MD simulations produce acceptable monomer ensembles. However, two different MD runs starting from random and PDB helix-rich initial conformations of Aβ_{40} result in two different structure distributions (with zero and 30% helix contents for most populated structures) nevertheless demonstrate excellent (0.98 and 0.96) correlation with the same experimental set of chemical shifts.[51] This result implies that the correlation factor cannot serve as a good indicator of reliability of *in silico* structural distributions. To understand this problem better we calculate the secondary chemical shift defined as $\Delta\delta = \delta - \delta_{RC}$, where δ_{RC} is a chemical shift for amino acids in random coil state. Using values of NMR δ_{RC} from Wishart *et al.*[55] one can show that the correlation coefficient between the experimental $\Delta\delta_{\text{exp}}$ and the simulation results obtained from the CMD run starting from PDB structure of Aβ_{40} is rather low, $R = 0.23$ (Fig. S5 in SM).[77] The better correlation $R = 0.37$ is observed for the MD simulation that initiates from random coil conformation, while the best fit with $R = 0.45$ has been found by REMD. The situation becomes different for Aβ_{42} as REMD gives worse correlation ($R = 0.30$) compared to the CMD ($R = 0.45$) (Fig. S5 in SM,[77] lower panel). Therefore, it is very difficult to reach good correlation with experiments on secondary chemical shifts even with the use of REMD. Nevertheless, our CMD presumably produces the structure ensemble of the same quality as REMD.

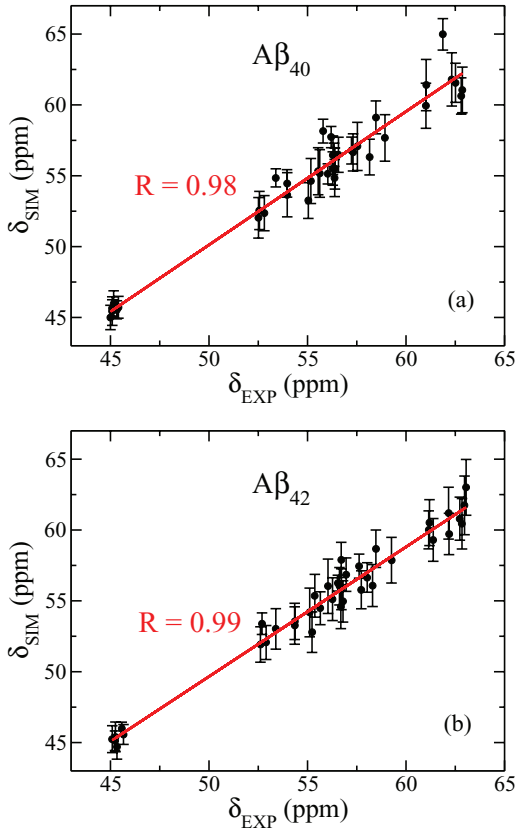

FIG. 2. Correlation between simulation and experimentally determined chemical shifts[51] for C_α atoms. δ_{sim} was estimated using the SHIFTS program, while δ_{exp} has been obtained by NMR method.[51] The data are collected for residues 2–39 for both Aβ_{40} and Aβ_{42}. Shown are results, obtained for monomer Aβ_{40} (a) and monomer Aβ_{42} (b).

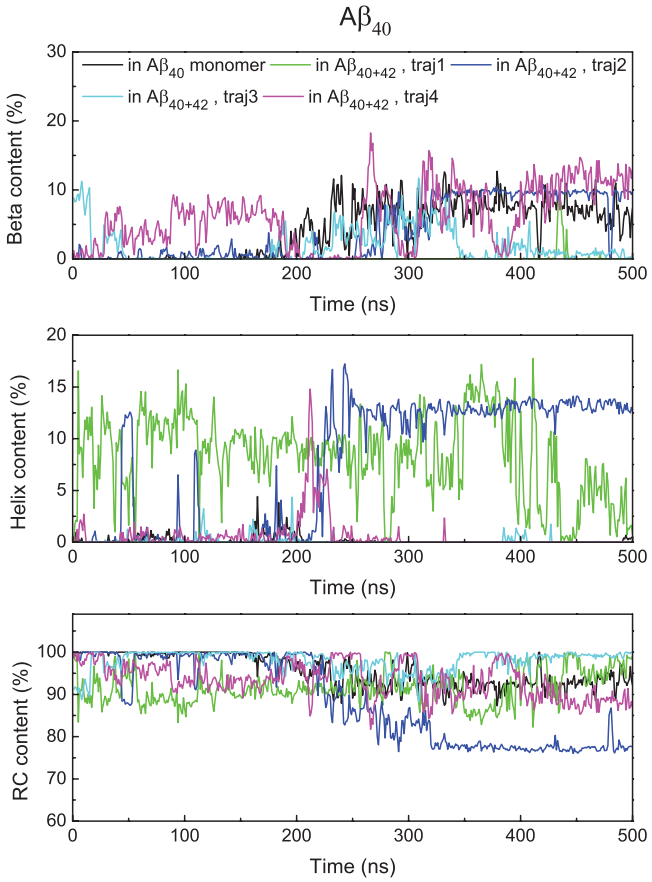

FIG. 3. Time dependence of the secondary structure content of Aβ_{40} in monomer (black lines), and first (green lines), second (blue), third (cyan), and fourth (magenta) trajectories of the di-peptide system. Result were averaged every 1 ns. The Stride's definition was used for computation of secondary structures.

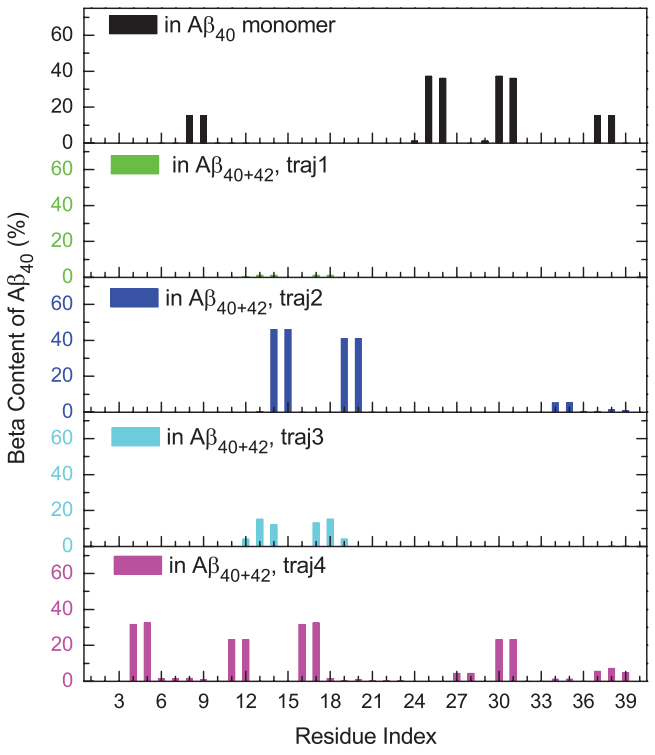

FIG. 4. Population of β-content of each residue of Aβ_{40} for monomer (black bar) and first (green), second (blue), third (cyan), and fourth (magenta) trajectories for the Aβ_{40+42} system. Results were obtained using the Stride's definition.

2. Secondary and tertiary structures of Aβ_{40} in monomer state

The time dependence of beta, helix, and *RC* contents of monomer Aβ_{40} is shown in Fig. 3 by black curves. The notable β-content occurs after about 150 ns, while helix structures remain very low during the whole run. Random coil structure is very high especially for first ≈150 ns. The β-structure occurs mainly at residues 8, 9, 25, 26, 30, 31, 37, and 38 (Fig. 4). The average value of beta, helix, and coil contents, obtained in equilibrium, is 5.2%, 0.2%, and 94.6%, respectively (Table I). With the help of a coarse-grained model, Vitalis and Caflisch[49] obtained the reasonable agreement with the CD estimates of 5% α-content and 25% β-content in aqueous buffer at 298 K.[56] However, one has to be cautious about this comparison because the experimental results have been obtained for Aβ_{10-35} fragment and there is no reason to believe that it has the same structure as full-length peptides. The UNRES force field provides much higher helix structures.[50] These results are different from our present results.

It seems that our simulations provide the α-content lower than previous all-atom replica exchange simulations with explicit[22] and implicit water.[20] Sgourakis *et al.* have used AMBER-derived PARM94, PARM96, MOD-PARM, GROMOS, and OPLS force fields, while an recently improved version of the AMBER force field PARM99SB has been employed by Yang and Teplow.[20] However, our β-content is compatible with the results reported by these groups. Using the C_α root mean square displacement (RMSD) conformational clustering method implemented in the GROMACS software and snapshots collected in equilibrium of 500 ns MD run one can obtain representative structures of monomer Aβ_{40} in aqueous environment. With the clustering tolerance of 1.0 Å we have obtained the most populated structure (84.2%) shown in Fig. 5 (upper panel). The typical snapshot of the second dominant cluster that has population 5.8% is shown in upper panel of Fig. S6 in SM.[77] This conformation is fully unstructured (100% *RC*). Thus, our results with poor beta structure (5.2%) and almost no helices (0.2%) (Table I) agree with the experiment of Zhang *et al.*[57] and Danielsson *et al.*[58] showing that the Alzheimer's Aβ peptide adopts a collapsed coil structure in water.[57]

3. Secondary and tertiary structures of Aβ_{42} in monomer state

As follows from Figs. 3 and 6 the β-content of Aβ_{42} in monomer state is markedly richer than that of Aβ_{40}. On average the β-content of Aβ_{42} (13.9%) (Table II) is about three times higher (compare with Table I). This is consistent with the experimental fact[21] that the former aggregates much faster than the latter one having higher population of fibril-prone state **N***. The similar result has been also reported in prior theoretical works.[20,22,36,59,60] Moreover, the C-terminal is rich in

TABLE I. Average secondary structures of Aβ_{40} peptide in monomer and dimer Aβ_{40+42} systems. The β-contents in disorder (1–8), β-strand 1 (8–23), loop (24–28), and β-strand 2 (29–40) regions are also given separately. *Region identifications for β-strands and loop are the same as in the work of Petkova et al.*[32] Results have been obtained using snapshots collected in equilibrium.

Content (%)	Region	Aβ_{40+42} Traj1	Aβ_{40+42} Traj2	Aβ_{40+42} Traj3	Aβ_{40+42}Traj4	Average	Monomer
	All (1–40)	0.1	4.7	1.6	6.5	3.2 ± 2.4	5.2
	Disorder (1–8)	0.0	0.0	0.0	8.5	2.1 ± 3.2	1.9
β	β-strand 1 (9–23)	0.3	11.6	4.3	7.7	6.0 ± 1.1	1.5
	Loop (24–28)	0.0	0.0	0.0	1.7	0.4 ± 0.6	14.8
	β-strand 2 (29–40)	0.0	1.1	0.1	5.5	1.7 ± 1.9	8.7
RC	All (1–40)	92.0	87.0	98.0	92.7	92.4 ± 2.9	94.6
Helix	All (1–40)	7.9	8.3	0.4	0.8	4.4 ± 3.8	0.2

β-contents (Fig. 7) having highly β-structured residues 37–40, while other theoretical studies show that β-structure is mainly located in region (38–41)[22] or (32–36).[20] This is in line with that the C-terminal is fibril-prone as observed in the experiment of Luhrs *et al.*[4] and the fibril growth of Aβ_{42} initiates by attaching to this terminal of peptides in the fibril forming a β-sheet on the fibril edge.[61]

Contrary to other theoretical studies, it was shown that the C-terminal is poorer in β-structure than the N-terminal[62] using the implicit solvent coarse-grained optimized potential for efficient structure prediction model (OPEP). It is not clear if this is due to drawbacks of coarse-graining or other reasons. The discrete MD coupled with the four-bead model has also predicted a β-strand in the N-terminus.[59] The β-content obtained in our simulations is slightly higher than that of Velez-Vega and Escobedo,[63] Yang and Teplow,[20] and Cote *et al.*[62] but significantly lower than the result reported by Mitternacht *et al.*[64] Such a high secondary structure, obtained by these authors, may be associated with omission of the electrostatic interaction in their force field.[65]

The α-structure of Aβ_{42} is poor remaining lower than 3% during the whole run (Fig. 6). The average α-content is 1.1% (Table II) which is a bit higher than Aβ_{40} (Table I). Our result

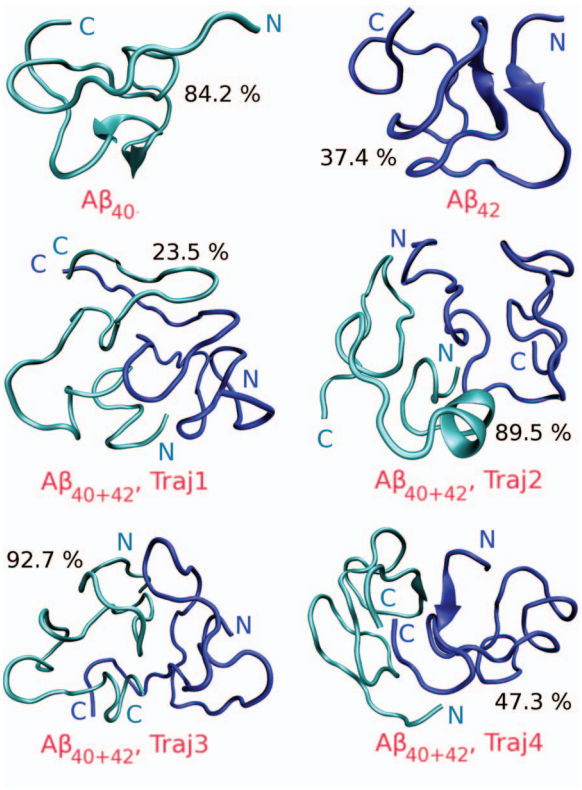

FIG. 5. Typical snapshots of the most populated clusters obtained by clustering technique with cutoff 1 Å. For monomer Aβ_{40} there are 90.0%, 0.0%, and 10.0% of *RC*, helix, and beta contents, respectively. For monomer Aβ_{42} one has 85.7%, 0.0%, and 14.3% of *RC*, helix, and beta content, respectively. In the case of first and third MD runs of the mixed system both peptides are entirely unstructured with 100% *RC*. (100% *RC* for both peptides). For trajectory 2 of the di-peptide complex, Aβ_{40} has 87.5%, 12.5%, and 0.0% of *RC*, helix, and beta content, respectively, while Aβ_{42} has 100% *RC*. In trajectory 4 both peptides have no helix structure. Aβ_{40} has 5% beta and 95% coil, whereas Aβ_{42} has 4.7% beta and 93.3% coil. The population of the first dominant clusters is shown next to structures.

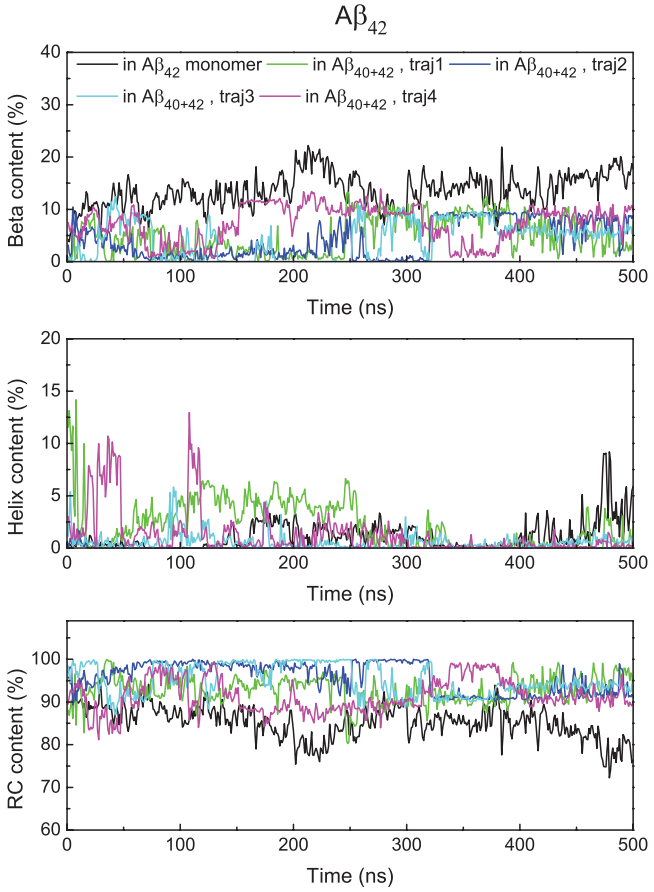

FIG. 6. The same as in Fig. 3 but for Aβ_{42}.

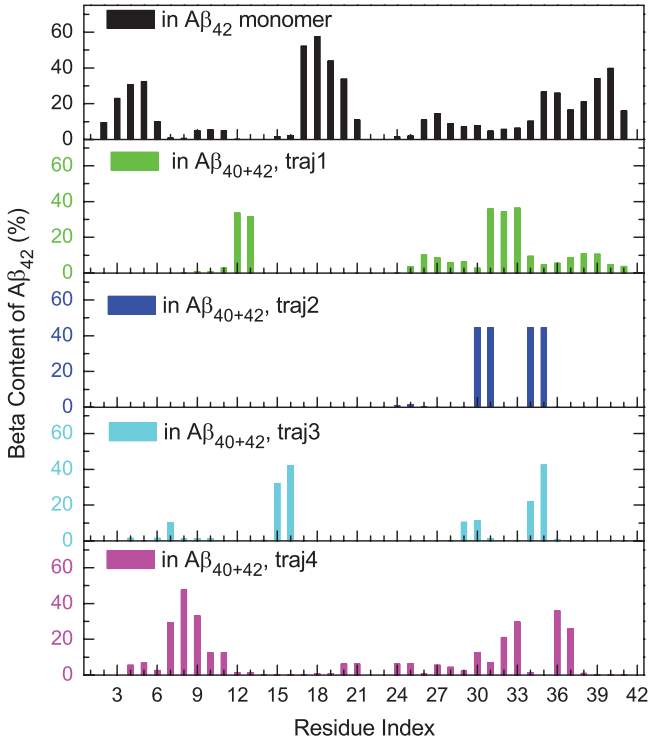

FIG. 7. Population of β-content of each residue of Aβ_{42} for the Aβ_{42} monomer (black bar), first (green), second (blue), third (cyan), and fourth (magenta) trajectory of Aβ_{40+42} system.

on helix structure of Aβ_{42} monomer is comparable with several groups,[62,63,66] but lower than that reported by Yang and Teplow.[20]

The *RC* varies between 75% and 85% (Fig. 6). In equilibrium the average value *RC* is 85.9% (Table II) implying that Aβ_{42} is more structured than Aβ_{40} which has 96.1% *RC* (Table I). Note that in our definition *RC* includes also turns as well as bends. Therefore our result is compatible with other groups.[20,22,62,63] The lower *RC* content has been obtained[64] using all-atom simulations with implicit water. Using the C_α RMSD conformational clustering method with tolerance of 1.0 Å, we have obtained the most populated structure (37.4%) shown in Fig. 5 (upper panel). This structure has 85.7%, 0.0%, and 14.3% of *RC*, helix, and beta content, respectively. The population of the second dominant cluster is 33.9% (Fig. S6 in SM,[77] upper panel). The first and second dominant clusters the same population of secondary structures but beta structures are located at different places (Fig. 5 and Fig. S6 in SM[77]).

B. Mixed system Aβ_{40+42}

1. Aβ_{40} in the di-peptide system

To study changes in structures of two peptides in the mixed system we have carried 4 MD runs of 500 ns. The time dependence of the energy, shown in Fig. S7 in SM,[77] shows that this system reaches equilibrium after $t_{eq} \approx 90$, 60, 115, and 70 ns for trajectory 1, 2, 3, and 4, respectively. We have estimated the specific heat for intervals $[t_{eq}, t_{full}/2]$ and $[t_{eq}, t_{full}]$ for four trajectories (Table S1 in SM[77]). The largest difference between two time windows, $\Delta C_P = 0.195$ kcal/(molK), is observed for trajectory 3. Since $\Delta C_P/C_P \approx 5\%$, the system reaches equilibrium for this trajectory. Averaging over 4 trajectories we have $C_P = 3.607 \pm 0.123$ and 3.634 ± 0.224 kcal/(molK) for the first and second windows, respectively. So with error bars the values of the specific heat coincide implying that the system is in approximate equilibrium after t_{eq}. The vdW interaction between Aβ_{40} and Aβ_{42} dominates over the electrostatic one (Fig. S8 in SM[77]).

β-structure occurs in the second (blue curve in Fig. 3) and fourth trajectory (magenta curve in Fig. 3) to greater extent than in the first and third ones. This is also evident from Fig. 4. After 300 ns of the second run the β-content does not fluctuate much. For this trajectory residues 14, 15, 19, and 20 are very rich in beta structure, while residues 4, 5, 11, 12, 16, 17, 30, and 31 dominate in run 4 (Fig. 4). Averaging over 4 trajectories we obtain the population of beta structures of Aβ_{40} in the complex system (Fig. S9 in SM[77]). Obviously, region (11–19), especially residues 14, 15, 19, and 20 (Fig. 4), is richer in β-structure than the remaining parts (Table I).

Overall, the presence of Aβ_{42} slightly reduces the β-content of Aβ_{40} from 5.2% in the monomer to 3.2% in the dimer (Table I). In the mixed system the helix content increases from 0.2% to 4.4% (Table I).

2. Aβ_{40} can interfere with aggregation of Aβ_{42}

The alternative way to study the inhibition of Aβ_{42} assembly by Aβ_{40} is to monitor the change in aggregation rates

TABLE II. Average secondary structures of Aβ_{42} peptide in monomer and dimer Aβ_{40+42} systems. The β-contents in disordered (1–16), β-strand 1 (17–26), loop (27–30), β-strand 2 (31–42), and two β-strands (17–26)+(31–42) regions are also given separately. *Region identifications for β-strands and loop are the same as in the work of Luhrs et al.*[4] Results have been obtained using snapshots collected in equilibrium.

Content (%)	Region	Aβ_{40+42} Traj1	Aβ_{40+42} Traj2	Aβ_{40+42} Traj3	Aβ_{40+42} Traj4	Average	Monomer
	All (1–42)	6.5	4.3	4.3	7.8	5.7 ± 1.4	13.9
	Disorder (1–16)	4.3	0.0	5.7	9.6	4.9 ± 2.8	7.9
β	β-strand 1 (17–26)	1.4	0.3	0.0	2.7	1.1 ± 1.0	21.3
	Loop (27–30)	5.9	11.4	5.5	6.2	7.2 ± 2.1	9.5
	β-strand 2 (31–42)	13.7	11.1	5.6	10.2	10.2 ± 2.3	17.2
	(17–26)+(31–42)	8.1	6.2	3.1	6.8	6.1 ± 1.8	19.1
RC	All (1–42)	91.4	95.7	95.2	91.4	93.2 ± 2.0	84.9
Helix	All (1–42)	2.1	0.0	0.5	0.8	0.9 ± 0.6	1.2

in the presence of the latter. Because this task is computationally prohibited for such long peptides as full-length Aβ peptides we try to get indirect evidences using the correlation between the population of the fibril-prone state **N*** and fibril formation rates.[19] As mentioned above, Aβ_{42} aggregate much faster than Aβ_{40} having higher population of **N*** in monomer state. This fact is supported not only by the present study but previous ones.[20,63,67,68] Another example is that a recent experiment[69] showed that the aggregation rate of Aβ_{40}-lactam[D23–K28], in which the residues D23 and K28 are chemically constrained by a lactam bridge, is nearly a 1000 times greater than in the wild-type. This is because the salt bridge constraint increases the population of the **N*** conformation in the monomer state.[70] The decisive role of population of this conformation in self-assembly has been also confirmed by simulations of short peptides using different all-atom models with explicit water[35] as well as off-lattice[71] and lattice models.[19]

In the presence of Aβ_{40} the β-content of Aβ_{42} is reduced in all of four MD runs (Fig. 6). It becomes even more pronounced if one considers individual residues (Fig. 7). Aβ_{40} substantially decreases the β-content in fibril-prone regions (17–21) and (37–40). In the second trajectory β-structure almost disappears in the wide region (1–29) (Fig. 6) but with substantial increase in residues 30, 31, 34, and 35. In the third MD run residues 15, 16, and 35 are highly structured. The enhancement of β-content appears in the N-terminal and residues 33, 36, and 37 in the fourth trajectory (Fig. 6). Averaging over 4 trajectories we obtain individual β-content for Aβ_{42} in the complex system (Fig. S10 in SM[77]). In the presence of Aβ_{40} the β-content of fibril-prone regions (17–21) and (36–42) is nearly reduced to zero, but some enhancement is seen in (30–35) fragment. The beta content of β-strand 1 (region 17–26) is reduced from 21.3% in the monomer to 1.1% in the dimer (Table II). In contrast, the β-strand 2 content (region 31–42) does not vary much.

Within error bars the average total β-content clearly drops from 13.9% in monomer system to 5.7% in the two-peptide system Aβ_{40+42} (Table II). The decrease in β-content is also visible from comparison of the most (Fig. 5) and second (Fig. S6 in SM[77]) populated structures obtained by the clustering technique for monomer and di-peptide systems. For the first dominant clusters Aβ_{42} has nonzero beta content (4.7%) in trajectory 4 only. For the second central clusters this peptide has 9.5% beta in trajectories 3 and 4 but populations of these clusters are rather low (Fig. S6 in SM[77]).

Since the loop region of Aβ_{42} is small and within error bars Aβ_{40} does not affect its β-content (Table II) one can focus on two β-strands of **N***. The β-content in these two regions drops from 19.1% in monomer state to 6.1% in dimer state (Table II). This reduction means that the population of **N*** is decreased leading to our main conclusion that, in agreement with the experiments,[16–18] Aβ_{40} can inhibit aggregation of Aβ_{42}. One may think that reduction of β-content by $19.1 - 6.1 = 13\%$ has minor effect on fibril formation rates. However, as has been shown in our previous work, the fibril formation time $\tau_{\text{fib}} \sim \exp(-cP_{N*})$,[19] where $c \approx 1$ is a constant and population of the fibril-prone state P_{N*} is measured in percents. Since the beta-content is proportional to P_{N*}, one can expect that its reduction by about 13% would result in increase of τ_{fib} by $\approx$ five orders of magnitude. This estimation is made using $c = 1$ followed from simple lattice models with 8-bead sequences.[19] For all-atom models with sequences of 42 amino acids constant c is presumably larger and the inhibitory effect becomes more pronounced. Thus the reduction of beta-content of about 13% is not marginal from this point of view.

The presence of Aβ_{40} does not affect helical structure of Aβ_{42} (Fig. 6) leaving the average α-content unchanged (Table II). However, the *RC* content increases (Fig. 6) from 85.9% to 93.2% (Table II). Taken together, in the mixed system Aβ_{42} becomes less ordered compared to the monomer case.

3. Side chain–side chain interaction between Aβ_{40} and Aβ_{42} is more important than HB one

To shed light on the nature of ordering of peptides in dimer, we have constructed the SC (Fig. 8) and HB (Fig. S11 in SM)[77] contact map using snapshots collected in four MD runs. Obviously, the hydrophobic interaction dominates over the HB one and this is in line with the NMR study of Aβ_{10-35} peptide of Zhang *et al.*[57] In the first trajectory, about 18 residues from two N-terminals prefer to stay together. The C-terminal of Aβ_{40} forms contacts with the middle part of Aβ_{42} but with lower probability. For the second trajectory, the situation becomes different as the N-end of Aβ_{40} has almost no contact with Aβ_{42} (Fig. 8). In the third MD run a few residues from C-terminals of two peptides show the strong interaction. Residues 1–16 of Aβ_{40} has high propensity to have contact with the loop region of Aβ_{42} (Fig. 8). For the fourth trajectory residues 33–39 of Aβ_{40} prefer to interact with not only C-terminal but also N-terminal of Aβ_{42}. Residues from loop region of Aβ_{40} have high affinity to be near the Aβ_{42} C-terminal. The difference between four contact maps reflects the complexity of the underlying free energy landscape of the dimer. The existence of the large number of local minima constitutes the diversity of structures and this may be consistent with the NMR experiment that the fibril structure depends on the precise details of growth conditions.[72]

The contact maps (Fig. 8 and Fig. S11 in SM[77]) do not show any interaction between the two CHC regions (17–21). This fact is in line with the scenario that Aβ_{40} interferes with Aβ_{42} aggregation because the strong interaction of these regions would stabilize Aβ_{42} leading to enhancement of fibril formation.

4. Salt bridge D23–K28

As mentioned above the salt bridge D23–K28 plays the important role in stabilization of the turn region. This bridge is not stable as its forming atoms are solvated,[70,73] but if one makes it stable by forming a bond, the loop will now be stable and will assist the peptide in forming a hairpin like structure leading to acceleration of the fibril formation process. The substantial enhancement of aggregation by constraining the salt bridge D23–K28 has been demonstrated

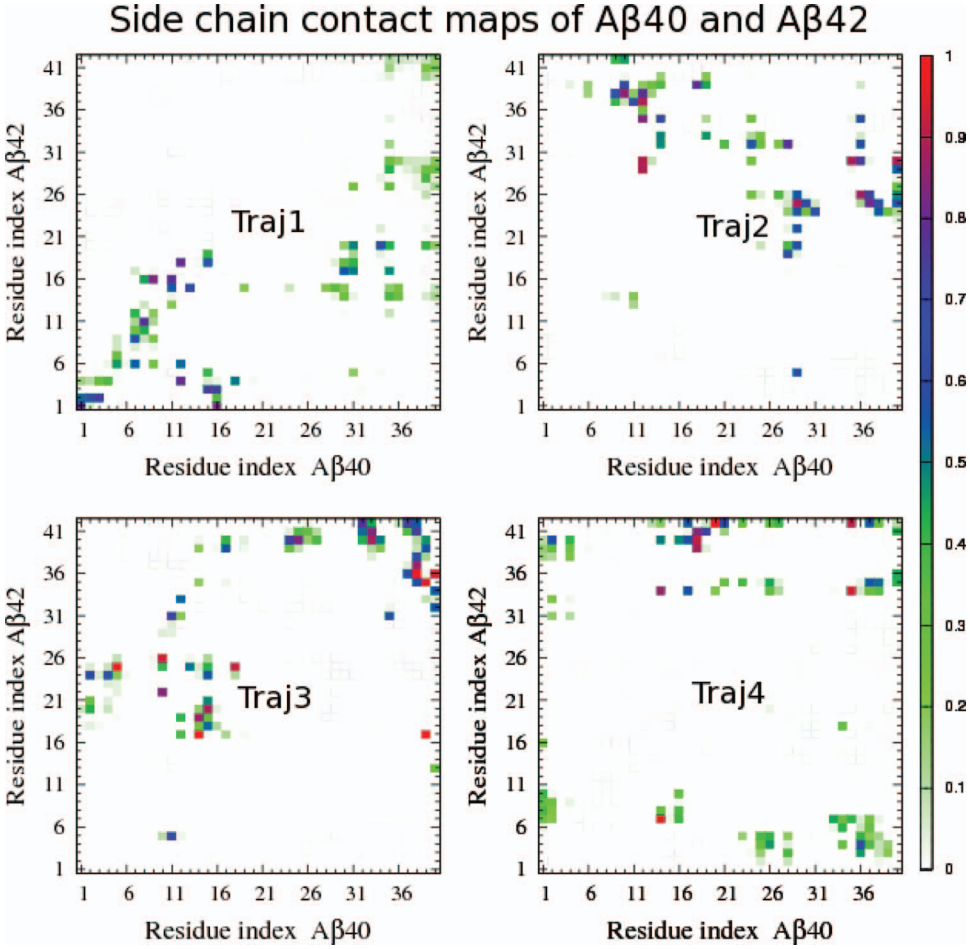

FIG. 8. Side chain contact map for Aβ_{40} and Aβ_{42} in the di-peptide system. Results were obtained for four trajectories in equilibrium.

experimentally.[69] Although a similar experiment has not been performed for Aβ_{1-42} yet, one can also expect that the increase in distance between D23 and K28 would interfere with fibrillogenesis of this peptide.

To monitor salt bridge flexibility we calculate the distance $d_{D23-K28}$ between atom C_γ of residue Asp23 and N_ζ of Lys28. As evident from the time dependence and distributions (Fig. 9), $d_{D23-K28}$ of Aβ_{42} in dimer is larger than in monomer state. This is true for all four MD trajectories performed for the Aβ_{40+42} complex. In the monomer case we have the average distance $d_{D23-K28} = 8.5$ Å, while $d_{D23-K28} = 12.3 \pm 2.1$ Å for dimer, where error bars come from averaging over 4 trajectories. The increase in $d_{D23-K28}$ is quite substantial, about 3.8 Å. Thus Aβ_{40} is expected to inhibit aggregation of Aβ_{42} as its presence makes the salt bridge of the latter more flexible.

The effect of Aβ_{42} on dynamics of the salt bridge of Aβ_{40} is demonstrated in Fig. S12 in SM.[77] In monomer state the average distance $d_{D23-K28} = 6.9$ Å. For the dimer case the visible effect is seen in trajectories 1, 2, and 4. Averaging over 4 trajectories we obtain $d_{D23-K28} = 8.5 \pm 1.0$ Å which is larger than the monomer value. Therefore, Aβ_{42} tends to interfere with aggregation of Aβ_{40} but this effect is presumably less pronounced compared to the influence of Aβ_{40} on Aβ_{42}.

5. Flexibility of fragment 18–33

It has been suggested that 18–33 fragment could nucleate Aβ folding and the formation of a bent structure within residues 22–28 could be the rate-limiting step in fibril formation.[43,46,74] We have computed C_α-RMSD of this fragment from its fibril-prone structure (Fig. S1 in SM[77]) for Aβ_{42} in monomer and di-peptide system (Fig. 10). For monomer we have average $RMSD = 7$ Å, whereas $RMSD = 7.8 \pm 0.3$ Å for dimer, where error bars come from averaging over 4 trajectories. Thus the presence of Aβ_{40} increases RMSD of 18–33 fragment of Aβ_{42} or reduces probability of existence of fibril-prone state **N***. This result supports the inhibitory mechanism of Aβ_{42} aggregation by Aβ_{40}.

We have also monitored time dependence of RMSD of Aβ_{40} (Fig. S13 in SM[77]). For monomer one has average $RMSD = 6.5$ and 6.4 ± 0.5 Å for monomer and dimer, respectively. Therefore within error bars RMSD of fragment 18–33 of Aβ_{40} remains unchanged in the presence of Aβ_{42}.

6. Estimation of binding free energy of Aβ_{40} to Aβ_{42} by MM-PBSA method

In order to calculate ΔG_{bind} we have used snapshots collected in equilibrium for four trajectories and the

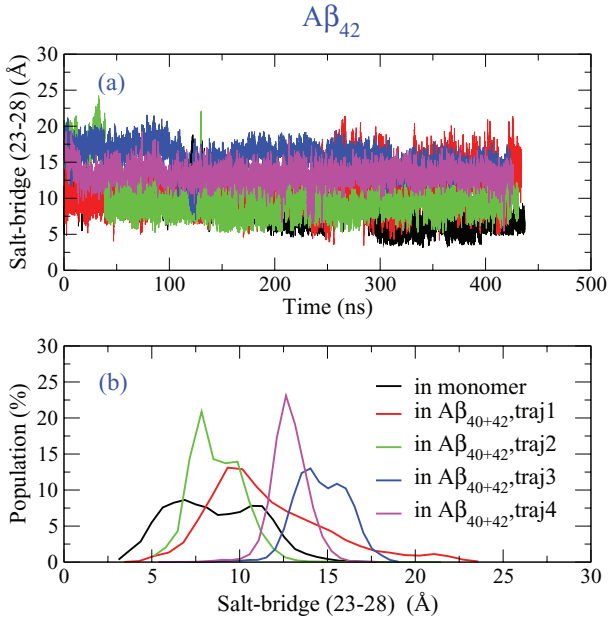

FIG. 9. Time dependence (a) and populations (b) of the distance between D23 and K28 of Aβ_{42}. Black curve refers to monomer while color curves refer to 4 trajectories of dimer. Averaging over the whole time window one has $d_{D23-K28} = 8.5$ Å for monomer, whereas $d_{D23-K28} = 12.0$, 9.0, 14.9, and 13.1 Å for trajectories 1, 2, 3, and 4 of dimer.

MM-PBSA method (see SM[77] for more details). The contribution of the vdW interaction is superior to the electrostatic one (Table III). For all trajectories the binding free energy is negative supporting good binding of Aβ_{40} to Aβ_{42}. Averaging over four MD runs we obtain $\Delta G_{\text{bind}} = -34.12 \pm 11.95$ kcal/mol. Thus, the underlying mechanism of inhibition lies in association of two peptides reducing the β-content or the population of **N*** conformation of Aβ_{42}. Our result is in good agreement with the experiment of Yang and Wang.[16]

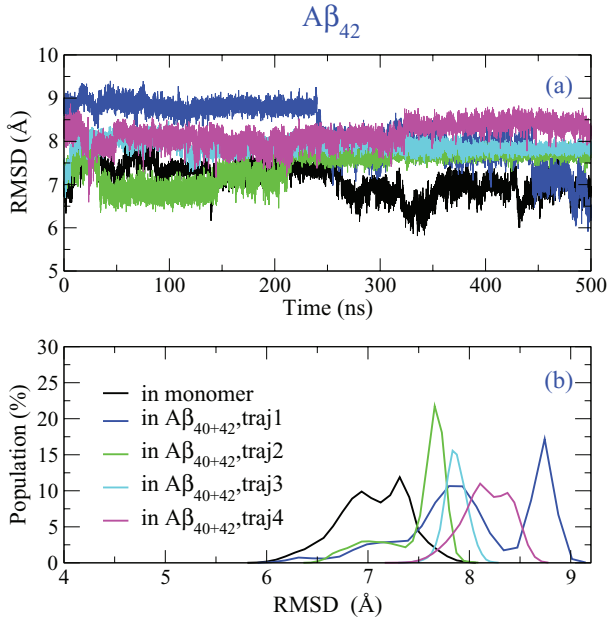

FIG. 10. The same as in Fig. 9 but for RMSD of fragment 18–33 from Aβ_{42} in monomer and complex systems. The corresponding fragment from fibril-prone structure has been used as the reference. The black curve denotes monomer while color curves refer to 4 trajectories of dimer. Averaging over the whole time window one has *RMSD* = 7Å for monomer, whereas *RMSD* = 8.1, 7.5, 7.9, and 7.7 Å for trajectories 1, 2, 3, and 4 of dimer.

TABLE III. Binding free energy of Aβ_{40} to Aβ_{42} in the di-peptide system. The data were obtained using snapshots collected in equilibrium (last 390, 440, and 430 ns for trajectory 1, 2, and 4, respectively (Fig. S7 in SM[77]) and the MM-PBSA method. *For third trajectory snapshots between 115 and 380 ns have been used skipping high energy structures from 380 to 500 ns.*[75] All quantities are measured in kcal/mol.

Aβ_{40+42}	ΔE_{vdW}	ΔG_{sur}	ΔE_{elec}	ΔG_{PB}	$-T\Delta S$	ΔG_{bind} (kcal/mol)
Traj1	−118.88	−13.80	−32.49	61.07	61.29	−42.81
Traj2	−83.20	−9.17	76.91	−59.58	54.57	−20.47
Traj3	−107.06	−12.46	36.73	−28.05	60.69	−49.75
Traj4	−84.35	−10.07	14.39	−5.53	59.45	−26.11
Average	−98.37	−11.38	23.89	−8.02	59.00	-34.12 ± 11.95

IV. CONCLUSION

As follows from Figs. 3 and 6 the β-structure occurs in Aβ_{42} much faster than in Aβ_{40}. Consistent with this finding, solvent conditions that facilitate the initial coil → β-structure transition would significantly accelerate fibril assembly. The N-terminal is less ordered than the C-one (Figs. 4 and 7) but not completely unstructured. This may be in line with the recent experiment showing that the English (H6R) and Tottori (D7N) mutations alter Aβ assembly at its earliest stages and produce oligomers that are more toxic to cultured neuronal cells than wild-type oligomers.[76] The experiments[17,18] have shown that the inhibition of Aβ_{42} fibrillogenesis by Aβ_{40} increases with increasing concentration of Aβ_{40} and the best inhibitory effect is achieved at stoichiometric ratio Aβ_{40}:Aβ_{42} ∼ 10:1.

However, the change in morphological properties of Aβ_{42} by the latter is observed in our simulations with ratio 1:1. This is presumably because the concentration used in our simulations (≈10 mM) is much higher than that used in experiments (∼1 μM).

In order to understand in more detail why the efficient inhibition happens at stoichiometric ratio Aβ_{40}:Aβ_{42} ∼ 10:1, we have calculated the binding free energy of Aβ_{42} to Aβ_{42}. We obtained $\Delta G_{\text{bind}} \approx -55.8$ kcal/mol (Viet and Li, unpublished results) that is lower than the binding free energy of Aβ_{40} to Aβ_{42} (Table III). This implies that Aβ_{42} peptides prefer to bind to each other more than to Aβ_{40} and one needs, therefore, high concentration of Aβ_{40} to observe pronounced inhibition.

We have shown that, in accord with the inhibitory mechanism, the presence of Aβ_{40} increases the beta content, distance between D23 and K28 of salt bridge and RMSD of 18–33 fragment of Aβ_{42}. Therefore these three quantities are sensitive indicators for studying Aβ_{42} aggregation.

We have shown that the protective role of Aβ_{40} is associated with preventing Aβ_{42} from aggregation. However, there is another possibility that Aβ_{40} can reduce toxicity by degrading oligomers or fibrils of Aβ_{42}. This question requires further investigation but our preliminary result on the binding

free energy suggests that Aβ_{40} can bind to Aβ_{42} aggregates and degrade them.

ACKNOWLEDGMENTS

The work was supported by Narodowe Centrum Nauki in Poland (Grant No. 2011/01/B/NZ1/01622) and Department of Science and Technology at Ho Chi Minh city, Vietnam. We are very thankful to M. G. Zagorski for providing experimental results on chemical shifts and D. B. Teplow and M. Yang for sharing their REMD data on structures of the most populated clusters of monomer systems. Allocation of CPU time at the supercomputer TASK in Gdansk (Poland) is highly appreciated.

[1] E. D. Eanes and G. G. Glenner, J. Histochem. Cytochem. **16**, 673 (1968).
[2] D. A. Kirschner, C. Abraham, and D. J. Selkoe, Proc. Natl. Acad. Sci. U.S.A. **83**, 503 (1986).
[3] A. T. Petkova, Y. Ishii, J. Balbach, O. Antzutkin, R. Leapman, F. Delaglio, and R. Tycko, Proc. Natl. Acad. Sci. U.S.A. **99**, 16742 (2002).
[4] T. Luhrs, C. Ritter, M. Adrian, D. Riek-Loher, B. Bohrmann, H. Doeli, D. Schubert, and R. Riek, Proc. Natl. Acad. Sci. U.S.A. **102**, 17342 (2005).
[5] K. N. Dahlgren, A. M. Manelli, W. B. Stine, L. K. Baker, G. A. Krafft, and M. J. LaDu, J. Chem. Biol. **277**, 32046 (2002).
[6] A. E. Roher, M. O. Chaney, Y. M. Kuo, S. D. Webster, W. B. Stine, L. J. Haverkamp, A. S. Woods, R. J. Cotter, J. M. Tuohy, G. A. Krafft, B. S. Bonnell, and M. R. Emmerling, J. Biol. Chem. **271**, 20631 (1996).
[7] M. Townsend, G. M. Shankar, T. Mehta, D. M. Walsh, and D. J. Selkoe, J. Physiol. **572**, 477 (2006).
[8] S. Lesne, M. T. Koh, L. Kotilinek, R. Kayed, C. G. Glabe, A. Yang, M. Gallagher, and K. H. Ashe, Nature (London) **440**, 352 (2006).
[9] J. Hardy and D. J. Selkoe, Science **297**, 353 (2002).
[10] R. Kayed, E. Head, J. L. Thompson, T. M. McIntire, S. C. Milton, C. W. Cotman, and C. G. Glabe, Science **300**, 486 (2003).
[11] B. Caughey and P. T. Lansbury, Annu. Rev. Neurosci. **26**, 267 (2003).
[12] M. Bentahir, O. Nyabi, J. Verhamme, A. Tolia, K. Horre, J. Wiltfang, H. Esselmann, and B. D. Strooper, J. Neurochem. **96**, 732 (2006).
[13] J. Theuns, E. Marjaux, M. Vandenbulcke, K. V. Laere, S. Kumar-Singh, G. Bormans, N. Brouwers, M. V. den Broeck, K. Vennekens, E. Corsmit, M. Cruts, B. D. Strooper, C. V. Broeckhoven, and R. Vandenberghe, Hum. Mutat. **27**, 888 (2006).
[14] J. Kim, L. Onstead, S. Randle, R. Price, L. Smithson, C. Zwizinski, D. W. Dickson, T. Golde, and E. McGowan, J. Neurosci. **27**, 627 (2007).
[15] I. Kuperstein, K. Broersen, I. Benilova, J. Rozenski, W. Jonekheere, M. Debulpaep, A. Vandersteen, I. Segers-Nolten, K. V. der Werf, V. Subramaniam, D. Braeken, G. Callewaert, C. Bartic, R. D'Hooge, I. C. Martins, F. Rousseau, J. Schymkowitz, and B. D. Strooper, EMBO J. **29**, 3408 (2010).
[16] Y. L. Yan and C. Y. Wang, J. Mol. Biol. **369**, 909 (2007).
[17] A. Jan, O. Gokce, R. Luthi-Carter, and H. A. Lashuel, J. Chem. Biol. **283**, 28176 (2008).
[18] M. M. Murray, S. L. Bernstein, V. Nyugen, M. M. Condron, D. B. Teplow, and M. T. Bowers, J. Am. Chem. Soc. **131**, 6313 (2009).
[19] M. S. Li, N. T. Co, C. K. Hu, J. E. Straub, and D. Thirumalai, Phys. Rev. Lett. **105**, 218101 (2010).
[20] M. Yang and D. B. Teplow, J. Mol. Biol. **384**, 450 (2008).
[21] S. W. Snyder, U. S. Ladror, W. S. Wade, G. T. Wang, L. W. Barrett, E. D. Matayoshi, H. J. Huffaker, G. A. Krafft, and T. F. Holzman, Biophys. J. **67**, 1216 (1994).
[22] N. G. Sgourakis, Y. L. Yan, S. A. McCallum, C. Y. Wang, and A. E. Garcia, J. Mol. Biol. **368**, 1448 (2007).
[23] B. Hess, C. Kutzner, D. van der Spoel, and E. Lindahl, J. Chem. Theory Comput. **4**, 435 (2008).
[24] B. Urbanc, M. Betnel, L. Cruz, G. Bitan, and D. B. Teplow, J. Am. Chem. Soc. **132**, 4266 (2010).
[25] A. Melquiond, X. Dong, N. Mousseau, and P. Derreumaux, Curr. Alzheimer Res. **5**, 244 (2008).
[26] S. Mitternacht, I. Staneva, T. Hard, and A. Irback, J. Mol. Biol. **410**, 357 (2011).
[27] S. Cote, R. Laghaei, P. Derreumaux, and N. Mousseau, J. Phys. Chem. B **116**, 4043 (2012).
[28] P. A. Kollman, I. Massova, C. Reyes, B. Kuhn, S. Huo, L. Chong, M. Lee, T. Lee, Y. Duan, W. Wang, O. Donini, P. Cieplak, J. Srinivasan, D. A. Case, and T. E. Cheatham, Acc. Chem. Res. **33**, 889 (2000).
[29] M. Coles, W. Bicknell, A. A. Watson, D. P. Fairlie, and D. J. Craik, Biochemistry **37**, 11064 (1998).
[30] S. Tomaselli, V. Esposito, P. Vangone, N. A. van Nuland, A. M. Bonvin, R. Guerrini, T. Tancredi, P. A. Temussi, and D. Picone, ChemBioChem **7**, 257 (2006).
[31] W. van Gunsteren, S. R. Billeter, A. A. Eising, P. H. Hünenberger, P. Krüger, A. E. Mark, W. Scott, and I. Tironi, *Biomolecular Simulation: The GROMOS96 Manual and User Guide* (Vdf Hochschulverlag AG an der ETH, Zurich, 1996).
[32] A. T. Petkova, W. M. Yau, and R. Tycko, Biochemistry **45**, 498 (2006).
[33] H. J. C. Berendsen, J. Postma, W. van Gunsteren, and J. Hermans, *Intermolecular Forces* (Reidel, Dordrecht, 1996).
[34] P. H. Nguyen, M. S. Li, G. Stock, J. E. Straub, and D. Thirumalai, Proc. Natl. Acad. Sci. U.S.A. **104**, 111 (2007).
[35] H. B. Nam, M. Kouza, H. Zung, and M. S. Li, J. Chem. Phys. **132**, 165104 (2010).
[36] M. H. Viet, S. T. Ngo, N. S. Lam, and M. S. Li, J. Phys. Chem. B **115**, 7433 (2011).
[37] R. W. Hockney, S. P. Goel, and J. Eastwood, J. Comput. Phys. **14**, 148 (1974).
[38] B. Hess, H. Bekker, H. J. C. Berendsen, and J. G. E. M. Fraaije, J. Comput. Chem **18**, 1463 (1997).
[39] T. Darden, D. York, and L. Pedersen, J. Chem. Phys. **98**, 10089 (1993).
[40] D. Frishman and P. Argos, Proteins: Struct., Funct., Genet. **23**, 566 (1995).
[41] M. Heinig and D. Frishman, Nucleic Acids Res. **32**, W500 (2004).
[42] J. P. Lee, E. R. Stimson, J. R. Ghilardi, P. W. Mantyh, Y. A. Lu, A. M. Felix, W. Llanos, A. Benhin, M. Cummings, W. Timms, and J. E. Maggio, Biochemistry **34**, 5191 (1995).
[43] N. D. Lazo, M. A. Grant, M. C. Condron, A. C. Rigby, and D. B. Teplow, Protein Sci. **14**, 1581 (2005).
[44] H. Y. Shao, S. C. Jao, K. Ma, and M. G. Zagorski, J. Mol. Biol. **285**, 755 (1999).
[45] C. J. Barrow, A. Yasuda, P. T. M. Kenny, and M. G. Zagorski, J. Mol. Biol. **225**, 1075 (1992).
[46] H. Sticht, P. Bayer, D. Willbold, S. Dames, C. Hilbich, K. Beyreuther, R. W. Frank, and P. Rosch, Eur. J. Biochem. **233**, 293 (1995).
[47] O. Crescenzi, S. Tomaselli, R. Guerrini, S. Salvadori, A. M. D'Ursi, P. A. Temussi, and D. Picone, Eur. J. Biochem. **269**, 5642 (2002).
[48] W. Humphrey, A. Dalke, and K. Schulten, J. Mol. Graphics **14**, 33 (1996).
[49] A. Vitalis and A. Caflisch, J. Mol. Biol. **403**, 148 (2010).
[50] A. Rojas, A. Liwo, D. Browne, and H. A. Scheraga, J. Mol. Biol. **404**, 537 (2010).
[51] L. Hou, H. Shao, Y. Zhang, H. Li, N. K. Menon, E. B. Neuhaus, J. M. Brewer, I.-J. L. Byeon, D. G. Ray, M. P. Vitek, T. Iwashita, R. A. Makula, A. B. Przybyla, and M. G. Zagorski, J. Am. Chem. Soc. **126**, 1992 (2004).
[52] X. P. Xu and D. A. Case, J. Biomol. NMR **21**, 321 (2001).
[53] X. P. Xu and D. A. Case, Biopolymers **65**, 408 (2002).
[54] V. Hornak, R. Abel, A. Okur, B. Strockbine, A. Roitberg, and C. Simmerling, Proteins **65**, 712 (2006).
[55] D. S. Wishart, C. G. Bigam, A. Holm, R. S. Hodges, and B. D. Sykes, J. Biomol. NMR **5**, 67 (1995).
[56] Y. Fezoui and D. B. Teplow, J. Biol. Chem. **277**, 36948 (2002).
[57] S. Zhang, K. Iwata, M. J. Lachenmann, J. W. Peng, S. Li, E. R. Stimson, Y. Lu, A. M. Felix, J. E. Maggio, and J. P. Lee, J. Struct. Biol. **130**, 130 (2000).
[58] J. Danielsson, J. Jarvet, P. Damberg, and A. Graslund, FEBS J. **227**, 3938 (2005).
[59] A. R. Lam, D. B. Teplow, H. E. Stanley, and B. Urbanc, J. Am. Chem. Soc. **130**, 17413 (2008).
[60] Y. S. Lin, G. R. Bowman, K. A. Beauchamp, and V. S. Pande, Biophys. J. **102**, 315 (2012).
[61] M. Han and U. H. E. Hansmann, J. Chem. Phys. **135**, 065101 (2011).
[62] S. Cote, P. Derreumaux, and N. Mousseau, J. Chem. Theory Comput. **7**, 2584 (2011).
[63] C. Velez-Vega and F. A. Escobedo, J. Phys. Chem. B **115**, 4900 (2011).
[64] S. Mitternacht, I. Staneva, T. Hard, and A. Irback, Proteins **78**, 2600 (2010).
[65] A. Irback and S. Mohanty, Biophys. J. **88**, 1560 (2005).
[66] N. G. Sgourakis, M. Merced-Serrano, C. Boutsidis, P. Drineas, Z. M. Du, C. Y. Wang, and A. E. Garcia, J. Mol. Biol. **405**, 570 (2011).

[67]K. H. Lim, H. H. Collver, Y. T. H. Le, P. Nagchowdhuri, and J. M. Kenney, Biochem. Biophys. Res. Commun. **353**, 443 (2007).
[68]Y. L. Yan and C. Y. Wang, J. Mol. Biol. **364**, 853 (2006).
[69]K. L. Sciarretta, D. J. Gordon, A. T. Petkova, R. Tycko, and S. C. Meredith, Biochemistry **44**, 6003 (2005).
[70]G. Reddy, J. E. Straub, and D. Thirumalai, J. Phys. Chem. B **113**, 1162 (2009).
[71]G. Bellesia and J.-E. Shea, J. Chem. Phys. **130**, 145103 (2009).
[72]A. K. Paravastu, I. Qahwash, R. D. Leapman, S. C. Meredith, and R. Tycko, Proc. Natl. Acad. Sci. U.S.A. **106**, 7443 (2009).
[73]B. Tarus, J. E. Straub, and D. Thirumalai, J. Am. Chem. Soc. **128**, 16159 (2006).
[74]Y. Chebaro, N. Mousseau, and P. Derreumaux, J. Phys. Chem. B **113**, 7668 (2009).
[75]Y. Miller, B. Y. Ma, and R. Nussinov, Proc. Natl. Acad. Sci. U.S.A. **107**, 9490 (2010).
[76]K. Ono, M. M. Condron, and D. B. Teplow, J. Biol. Chem. **285**, 23184 (2010).
[77]See supplementary material at http://dx.doi.org/10.1063/1.4730410 for the MM-PBSA method and additional figures.